Journal of Radioanalytical and Nuclear Chemistry (2025) 334:2981–2989
https://doi.org/10.1007/s10967-025-10020-6

Benchmarking of the PHITS simulation code using neutron activation experiments for reliable calculations of neutron fields

Doruntin Shabani[1,2,3] · Srinivasa T. Rangaiah[1] · Christoph Langer[1] · Eric Mauerhofer[3] · Paul Zakalek[3] · Thomas Gutberlet[3]

Received: 20 December 2024 / Accepted: 31 January 2025 / Published online: 15 February 2025

Abstract
In this study, experimental results from neutron activation of gold and indium foils are compared with the activation simulated using PHITS and PHITS-DCHAIN codes. The aim was to evaluate the accuracy of these simulation methods for predicting the amount of induced activity in such foils. Neutron activation experiments were carried out using a 10 Ci AmBe source at the University of Applied Sciences Aachen in Germany. Activities were determined using a modern BEGe detector by measuring the γ-ray spectra of decaying ^{198}Au and ^{116m}In. In the simulation, two methods were used to extract the activities: a direct flux analysis and a more detailed DCHAIN calculation. Generally, very good agreement of the activities within 15% is observed, which shows the reliable nuclear physics input and neutron transport calculation of the PHITS code for these kinds of experiments.

Keywords Activation method · Benchmarking · Validation · PHITS · ^{197}Au(n,γ)^{198}Au · ^{115}In(n,γ)$^{116\ mIn}$

Introduction

Neutrons play a pivotal role in modern science and technology. Since a long time, they are used in a wide variety of applications and fundamental research experiments. The free neutron has a lifetime of only about 15 min, which requires a constant neutron production to carry-out experiments and industrial applications. Ongoing effort is made to engineer reliable neutron sources based on very different production mechanisms, like fission, spallation or nuclear reactions. A typical example using nuclear reactions is a modern accelerator-driven compact neutron source (CANS), which attracted more and more interest over the past years [1, 2]. Especially the ability to keep the neutron source compact while producing strong neutron fields is a direct output of modern accelerator designs and technologies. The produced neutron field can be tailored to an individual application depending on the use case. This involves parameters such as neutron flux, neutron energy and angular distributions, extraction efficiencies, and brilliance. With this modern approach, it is possible to design neutron energies suited for neutron scattering experiments at cold neutron energies, but also thermal and epithermal fields for e.g. isotope production and even future medical therapy applications like boron neutron capture therapy [3, 4].

For the huge range of individual designs, it is important to make use of reliable tools for simulating the production of the neutrons and the resulting neutron field. This allows for a detailed extraction of desired parameters like energy and angular distributions. These tools need to cover the chain from production of the neutrons via the initiated nuclear reactions to the moderation and reflection process in a target-moderator-reflector system. Typically, modern Monte-Carlo simulations, which include nuclear reactions and moderating processes, are employed for these tasks [5, 6].

One of the general tools commonly used for such simulations is the Particle and Heavy Ion Transport code System (PHITS) [7]. Given the outlined importance of these simulations, it is necessary to assess their reliability and identify the parameters influencing the accuracy of the results.

✉ Doruntin Shabani
shabani@fh-aachen.de

[1] FH Aachen University of Applied Sciences, Campus Jülich, 52428 Jülich, Germany

[2] University of Cologne, 50937 Cologne, Germany

[3] Jülich Centre for Neutron Science, Forschungszentrum Jülich GmbH, 52425 Jülich, Germany

It is therefore important to benchmark the results of these PHITS simulations by comparing them to the results of measurements. A traditional method to determine properties of a neutron field is the neutron activation analysis (NAA) [8]. In this paper, we perform detailed simulations of a NAA employing the PHITS code. The simulations implement the properties and the environment of an americium-beryllium (AmBe) source at the University of Applied Sciences Aachen in Germany, to simulate the activation of gold and indium foils. Two different simulation methods are used to extract the activity of the foils at the end of the irradiation. Experimentally, both foils were activated using the existing experimental site and are subsequently analysed by using γ-ray spectroscopy. By comparing the experimental results with the simulated outcome, we benchmark the output of the PHITS code and therefore examine the reliability of PHITS for these kinds of applications. Finally, this study aims to provide insights into the accuracy of PHITS simulations and their applicability in neutron activation analysis.

In the following chapter, the experiment and the extraction of the activity of both foils is described. This is followed by a detailed discussion of the corresponding PHITS simulation and the derivation of the activity using two different methods. In the final chapter, both results are compared and evaluated in detail.

Experiment

High purity (> 99.8%) gold (m = 165 mg, S = 2.5 × 1.4 cm^2) and indium (m = 4.9 mg, S = 0.5 × 0.5 cm^2) foils of 0.025 mm thickness were irradiated at the irradiation facility of the Aachen University of Applied Sciences depicted in Fig. 1. It consists of an americium-beryllium (AmBe) sealed neutron source surrounded by a paraffin wax cube with sides of 71 cm. The cube is lined with 0.5 cm thick successive layers of Fe, Cd and Fe. Five plexiglass tubes with a length of 49 cm, an inner diameter of 2 cm and a wall thickness of 0.5 cm are inserted in the middle of the paraffin wax cube. The AmBe source was placed at the bottom of the central tube. The activity of the source was 370 GBq and the neutron emission specified by the supplier is $(2.0 \pm 0.2) \times 10^7$ s^{-1}. The foils were fixed on the inner wall of a polyethylene cup, which was positioned at the height of the neutron source for irradiation (see Fig. 1).

The irradiation time was 7 h for gold and 2 h for indium. The activities of ^{198}Au ($T_{1/2}$ = 2.69 d) and ^{116m}In ($T_{1/2}$ = 54.3 min) induced by neutron capture on ^{197}Au and ^{115}In were determined using a Broad Energy Germanium (BEGe, Mirion Technologies) detector with of relative efficiency of 34%. The gamma spectra of the gold and indium foils were measured for 67 and 26 h after waiting times of 69 and 0.1 h from the end of the irradiation, respectively. The distance between the foil and the detector end cap was 19 cm for gold and 0 cm for indium. The measured spectra are shown in Figs. 2 and 3. The GENIE 2000 software V3.4.1. (Mirion Technologies) [9] was used to analyse the recorded spectra. Calibration of the BEGe detector in energy, resolution i.e. full width at half maximum (FWHM) and efficiency i.e. full-energy-peak (FEP) efficiency was performed with ^{152}Eu and ^{137}Cs point sources of well-known activities. For the determination of the FEP efficiency at 0 cm losses due to true coincidence summing were corrected using the method given in [10]. The dependence of the FEP-efficiency $\varepsilon_{E\gamma}$ on the gamma-ray energy E_γ for the two measurement positions is shown in Fig. 4. and can be expressed for the energy range 121–1400 keV by the following expression:

$$ln(\varepsilon_{E\gamma}) = \sum_{i=0}^{4} a_i \left(ln(E_\gamma)\right)^i \quad (1)$$

with $a_0 = -1.181798\ 10^2$, $a_1 = 7.576702\ 10^1$, $a_2 = -1.869284\ 10^1$, $a_3 = 2.013540$ and $a_4 = -8.092704\ 10^{-2}$ for the distance of 19 cm, $a_0 = -1.215370\ 10^2$, $a_1 = 8.133236\ 10^1$, $a_2 = -2.029289\ 10^1$, $a_3 = 2.211086$ and $a_4 = -8.983246\ 10^{-2}$ for the distance of 0 cm and E_γ in keV.

The activity A (Bq) of ^{198}Au and ^{116m}In produced at the end of the irradiation was calculated using the following relation:

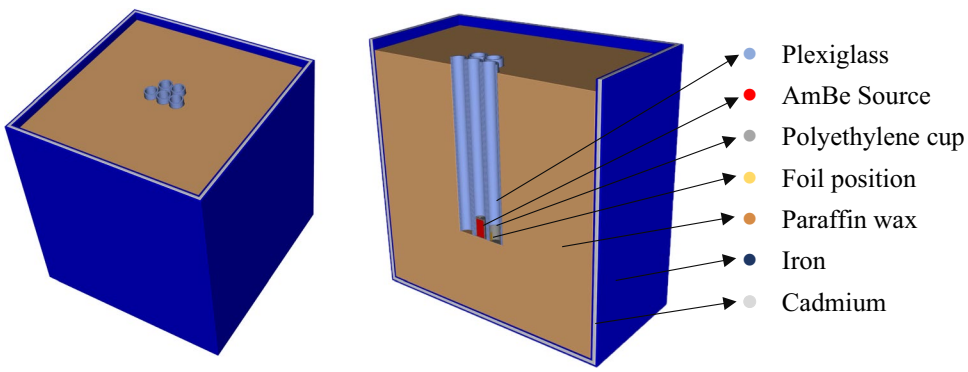

Fig. 1 Geometrical model of the irradiation facility used for the simulations. Left picture: view from the top. Right picture: vertical cut in the middle plane along the symmetry axis of the Plexiglas tube containing the AmBe source with the material description

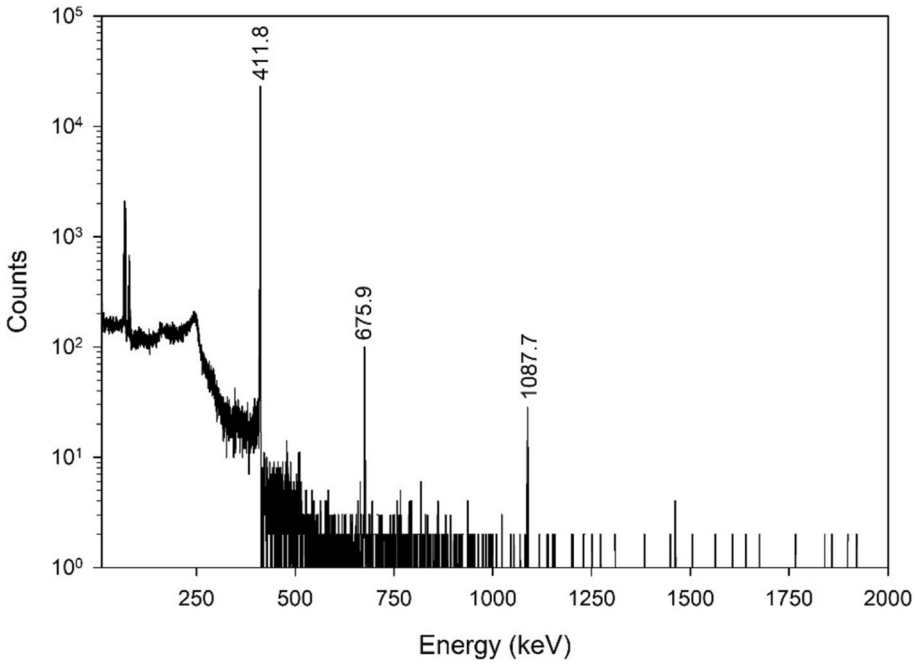

Fig. 2 Gamma-ray spectra of the gold foil (m = 0.165 g) recorded for 67 h after an irradiation time of 7 h and a waiting time of 69 h from the end of irradiation. The gamma lines of ^{198}Au are labelled on the spectrum. Non-labelled lines are background lines

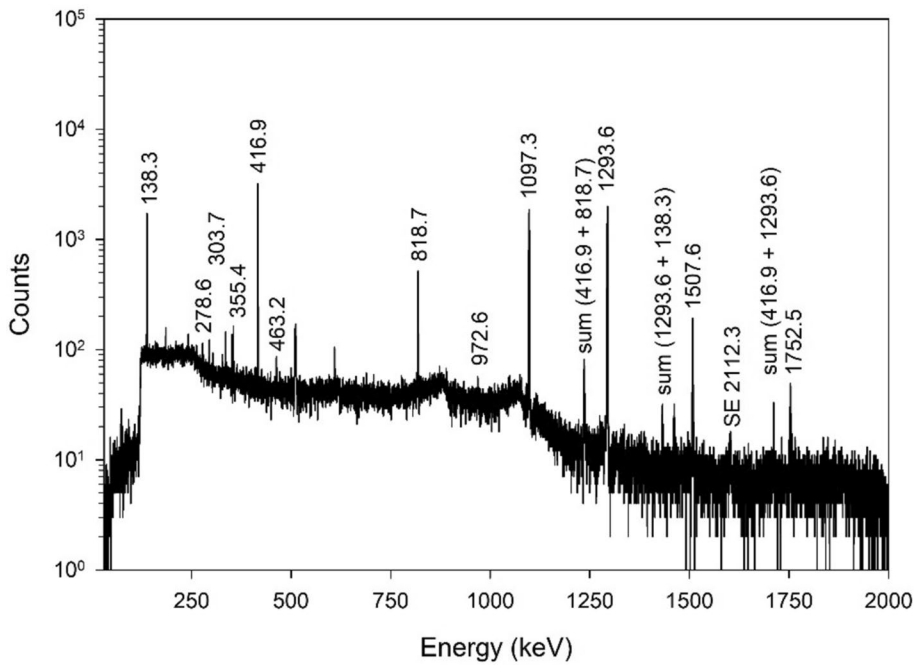

Fig. 3 Gamma-ray spectra of the indium foil (m = 0.0049 g) recorded for 26 h after an irradiation time of 2 h and a waiting time of 0.1 h from the end of irradiation. The gamma lines of ^{116m}In including summation peak due to true coincidences are labelled on the spectrum. Non-labelled lines are background lines

$$A = \frac{P_{E_\gamma} \cdot \lambda}{\varepsilon_{E_\gamma} \cdot I_{E_\gamma} \cdot \left(1 - e^{-\lambda \cdot t_m}\right) \cdot e^{-\lambda \cdot t_d}} \quad (2)$$

where P_{E_γ} is the net peak area of the gamma line at energy E_γ, λ [s^{-1}] the decay constant of the considered isotope, t_m [s] the counting (live) time, ε_{E_γ} the FEP efficiency, I_{E_γ} the intensity of the gamma ray and t_d [s] is the waiting time between the end of the irradiation and the start of the measurement. The activity of ^{198}Au was calculated from the 411-keV line and this of ^{116m}In from the 417-, 1097- and 1293-keV lines. The results are given in Table 1.

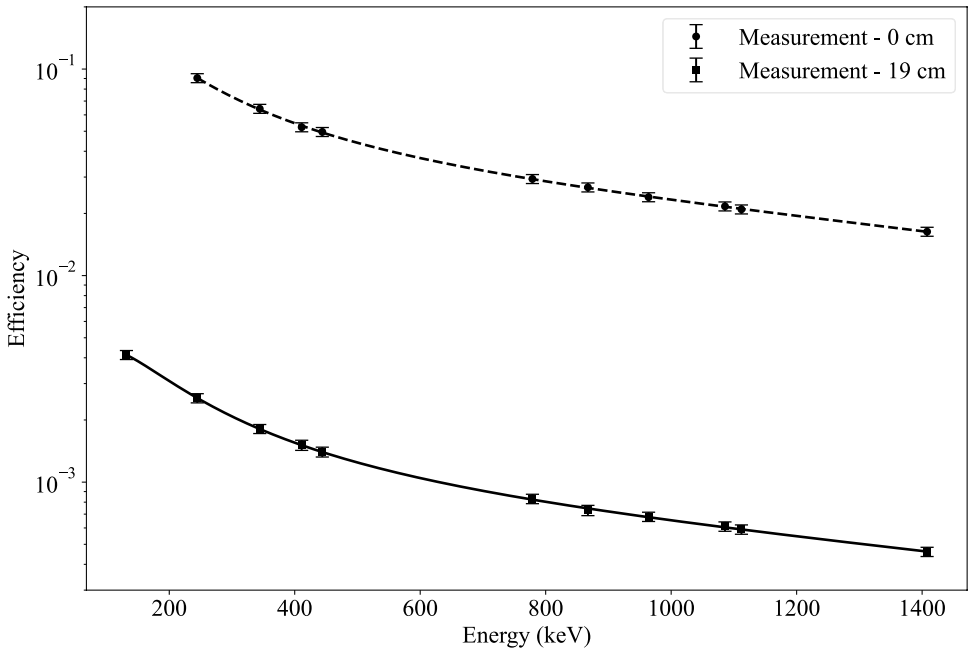

Fig. 4 Energy dependence of the full-energy-peak efficiency (FEP-efficiency) for the two measurement distances of the foils from the detector end-cap, 0 and 19 cm. The dashed lines represent the fit of the data with Eq. (1)

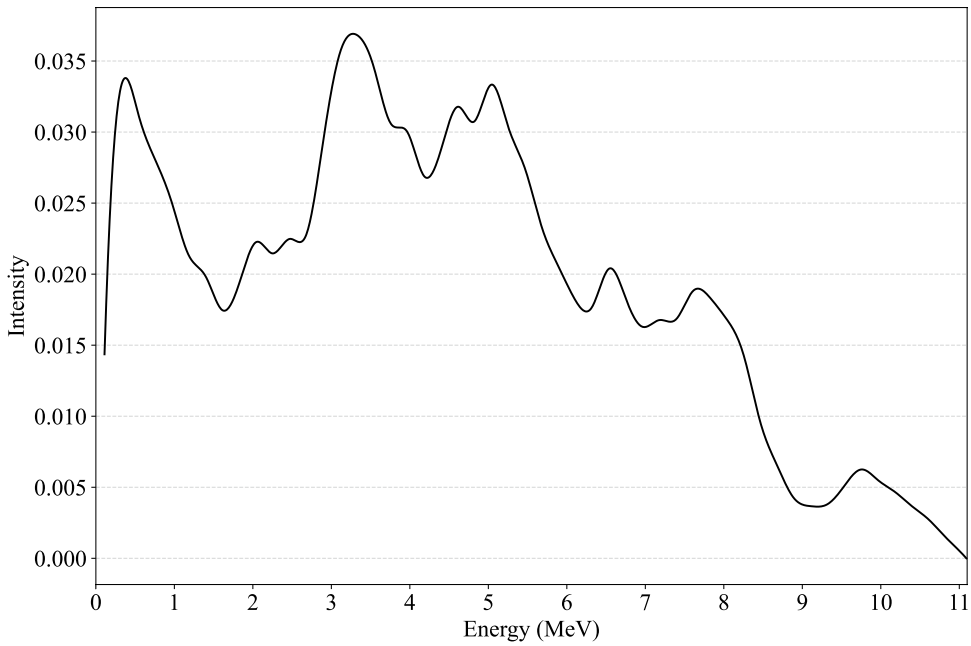

Fig. 5 Neutron energy spectrum used to simulate the AmBe source utilized in the experiment. The spectrum data were derived from PHITS supplementary files [8]

Table 1 Obtained net counts and the parameters used for the calculation of activity foils

Foils	Reaction	$T_{1/2}$	E_γ [keV]	$I_{E\gamma}$ (%)	$\varepsilon_{E\gamma}$	$P_{E\gamma}$	A (Bq)
Au	$^{197}Au(n, \gamma)^{198}Au$	2.6948 d	411.2	95.62	0.00151	29,887 ± 173	238 ± 24
In	$^{115}In(n, \gamma)^{116m1}In$	54.29 min	416.9	27.2	0.0524	12,796 ± 112	206 ± 21
			1097.3	58.5	0.0213	11,018 ± 108	203 ± 20
			1293.6	84.8	0.018	13,197 ± 122	199 ± 20

The intensity of the gamma ray ($I_{E\gamma}$) taken from [11]

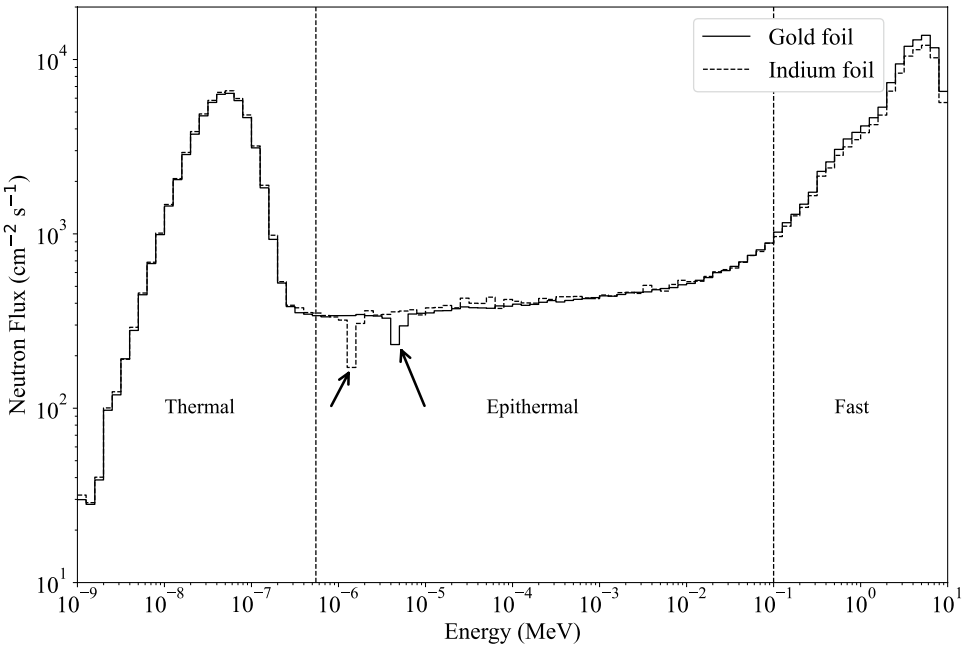

Fig. 6 Neutron energy spectra within the gold and indium foils obtained from the simulations. The arrows indicate the neutron flux depression at the resonance energy of 1.46 eV for ^{115}In and 4.90 eV for ^{197}Au

Simulation

In order to determine the activity of the foils the neutron energy spectra within the foils were simulated with the Monte Carlo code PHITS (Particle and Heavy Ion Transport code Sytem, version 3.22) [7] using the nuclear data library JENDL 4.0 [12]. Additionally, the activity of ^{198}Au and ^{116m}In was determined with DCHAIN [13], which is a module of PHITS allowing the direct calculation of the activity. In this method the neutron energy spectra within the foil with 1968 energy group structure (distributed into 1968 individual energy groups) below 20 MeV as a basic input file for DCHAIN, is produced. Then DCHAIN, which contains the neutron activation cross sections with 1968 group structure, is executed producing the activity of the foil. The geometrical model of the irradiation facility used for the simulations is as shown in Fig. 1. The simulations were performed with 10^9 source particles. The neutron energy spectra within the gold and indium foils are given in Fig. 6. The depression of the neutron flux at the energy of the main resonances, indicated by arrows, of gold (4.90 eV) and indium (1.46 eV) can be well observed.

The spectra are divided into three energy regions defined as thermal (1 meV to 0.5 eV), epithermal (0.5 eV to 0.1 MeV) and fast (0.1 MeV to 10 MeV). In the thermal energy region, the neutrons are in thermal equilibrium with the surrounding medium and their velocities conform the Maxwell–Boltzmann distribution with the neutron capture cross sections being inversely proportional to the neutron velocity [14].

In the epithermal region, the neutron capture cross-sections display resonances and the neutron flux is related to the neutron energy in a specific way. The dependence of the neutron flux $\boldsymbol{\phi_{epi}(E)}$, on the neutron energy E in this region can be expressed by:

$$\boldsymbol{\phi_{epi}(E)} = \frac{\boldsymbol{\phi_{epi}}}{\boldsymbol{E}^{1+\alpha}} \tag{3}$$

where $\boldsymbol{\phi_{epi}}$, is the epithermal neutron flux at an energy of 1 eV and α a parameter accounting for deviation from an ideal 1/E epithermal neutron spectrum. Integration of Eq. (3) over the energy limits E_{min} and E_{max} leads to

$$\boldsymbol{\phi_{epi}} = \frac{\boldsymbol{\phi_{tot}} \cdot \boldsymbol{\alpha}}{(\boldsymbol{E_{min}^{-\alpha}} - \boldsymbol{E_{max}^{-\alpha}})} \tag{4}$$

where $\boldsymbol{\phi_{tot}}$ is the total epithermal neutron flux for the energy range $E_{min} = 0.5$ eV, to $E_{max} = 0.1$ MeV. If the neutron flux, $\boldsymbol{\phi_{epi}(E)}$ can be obtained over small energy intervals $\boldsymbol{\Delta E}$, the interval gives an average flux value in that range, such as

Table 2 Thermal, epithermal and fast neutron flux within the gold and indium foils and α parameters determined from the simulated neutron energy spectra shown in Fig. 5

Foil	α	$\boldsymbol{\phi_{th}}$(cm^{-2} s^{-1})	$\boldsymbol{\phi_{epi}}$(cm^{-2} s^{-1})	$\boldsymbol{\phi_{fast}}$(cm^{-2} s^{-1})
Au	-0.066 ± 0.0066	$(5.11 \pm 0.51) \times 10^4$	$(1.30 \pm 0.13) \times 10^3$	$(1.10 \pm 0.11) \times 10^5$
In	-0.067 ± 0.0067	$(5.26 \pm 0.53) \times 10^4$	$(1.33 \pm 0.12) \times 10^3$	$(9.80 \pm 0.11) \times 10^4$

Table 3 Parameters used to calculate the ^{198}Au and ^{116}In activities A_{Flux} at the end of the irradiation by means of Eq. (6). The neutron fluxes are given in Table 2

Foil	Reaction	σ_{th}(b)	I_γ(b)	σ_{fast}(b)	E_r (eV)	$I_\gamma(\alpha)$(b)	$A_{Flux\ Analysis}$ (Bq)	A_{DCHAIN} (Bq)
Au	^{197}Au(n, γ)^{198}Au	98.7 ± 0.1	1550 ± 28	0.05 ± 0.04	5.65 ± 0.40	1738 ± 35	275 ± 28	207 ± 21
In	^{115}In(n, γ)^{116m}In	161 ± 3.2	2705 ± 76	0.10 ± 0.01	1.56 ± 0.03	2972 ± 52	238 ± 24	196 ± 20

A_{DCHAIN} is the activity returned by the DCHAIN module of the PHITS code. Thermal neutron cross section (σ_{th}), resonance integral (I_γ), and effective resonance energy (E_r) are obtained from [15]. Fast neutron cross section (σ_{fast}) is determined from the convolution of the reaction cross section from JENDL 4.0 library [12] obtained from [16] with the fast neutron spectrum given in Fig. 6 (100 keV to 10 MeV)

$$ln\left(\frac{\phi_{epi}(E)}{\Delta E}\right) = -(1+\alpha)\cdot \ln(E) \tag{5}$$

The analysis of the epithermal region of the neutron energy spectra shown in Fig. 6 with Eq. (5) lead to a parameter α of -0.066 for the gold foil and -0.067 for the indium foil. The thermal, epithermal and fast neutron fluxes within the foils are given in Table 2.

The activity **A** (Bq) at the end of the irradiation is calculated by:

$$A = \frac{m}{M}\cdot N\cdot h\cdot\left(\sigma_{th}\cdot\phi_{th}+I_\gamma\cdot\phi_{epi}+\sigma_{fast}\cdot\phi_{fast}\right)\cdot\left(1-e^{-\frac{ln2\cdot t_b}{t_{1/2}}}\right) \tag{6}$$

where m (g) is the mass of the element, N is the Avogadro's number, M (g/mol) the molar mass, h the abundance of the isotope, t_b (s) the irradiation time, $t_{1/2}$ (s) the half-life of the radionuclide, σ_{th} (cm^2) and σ_{fast} (cm^2) the thermal and fast neutron cross-section, I_γ (cm^2) the radiative neutron capture resonance integral, and ϕ_{th}, ϕ_{epi} and ϕ_{fast} (cm^{-2}s^{-1}) the thermal, epithermal and fast neutron flux within the sample. The radiative neutron capture resonance integral can be expressed as a function of α by [14]:

$$I_\gamma(\alpha) = \left(\frac{I_\gamma - 0.426\cdot\sigma_{th}}{{E_r}^\alpha} + \frac{0.426\cdot\sigma_{th}}{(2\cdot\alpha+1)\cdot{E_{Cd}}^\alpha}\right)\cdot 1eV^\alpha \tag{7}$$

where E_r, is the effective resonance energy for the considered (n, γ) reaction, and E_{Cd}, the cadmium cut-off energy. Equation 7 only holds when $E_{Cd} = 0.55$ eV, since $2(E_0/E_{Cd})^{1/2} = 0.426$ with $E_0 = 0.025$ eV. Cross sections, resonance integrals and effective resonance energies for the ^{197}Au(n, γ)^{198}Au and ^{115}In(n, γ)^{116m}In reactions are given together with the activities calculated by means of Eqs. (6) and (7) and returned by the DCHAIN module of the PHITS code in Table 3.

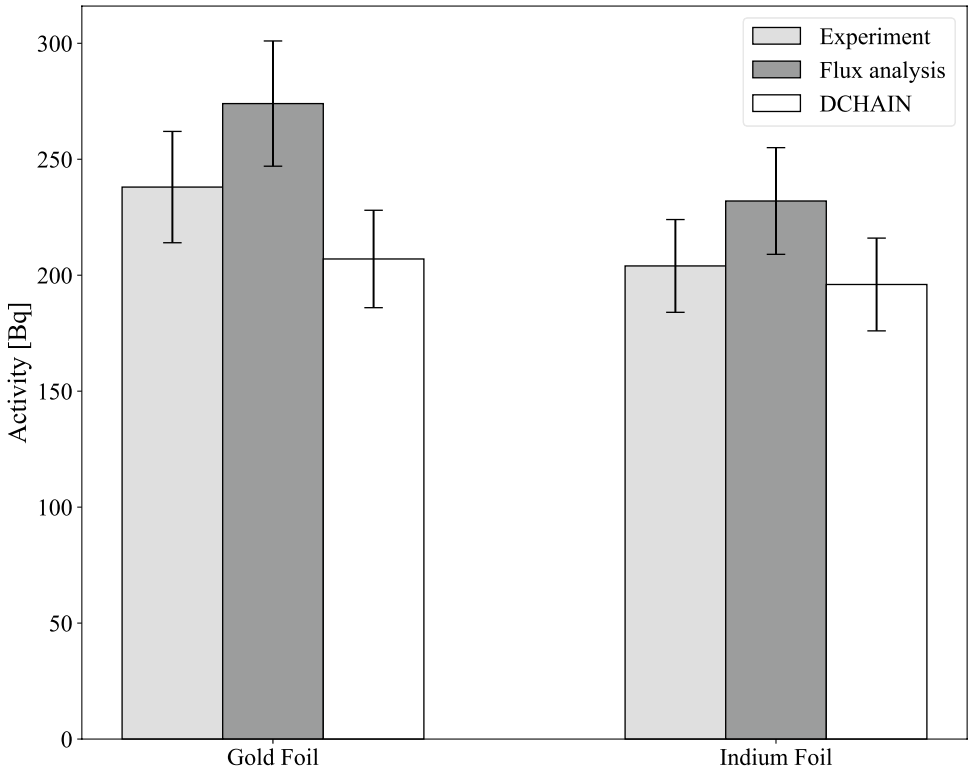

Fig. 7 Measured and simulated ^{198}Au and ^{116m}In activity at the end of the irradiation of the gold and indium foils. Flux analysis method: the activity is calculated by means of Eq. (3) using the thermal, epithermal and fast neutron flux simulated within the foils with PHITS. PHITS-DCHAIN method: the activity is directly calculated from the DCHAIN module

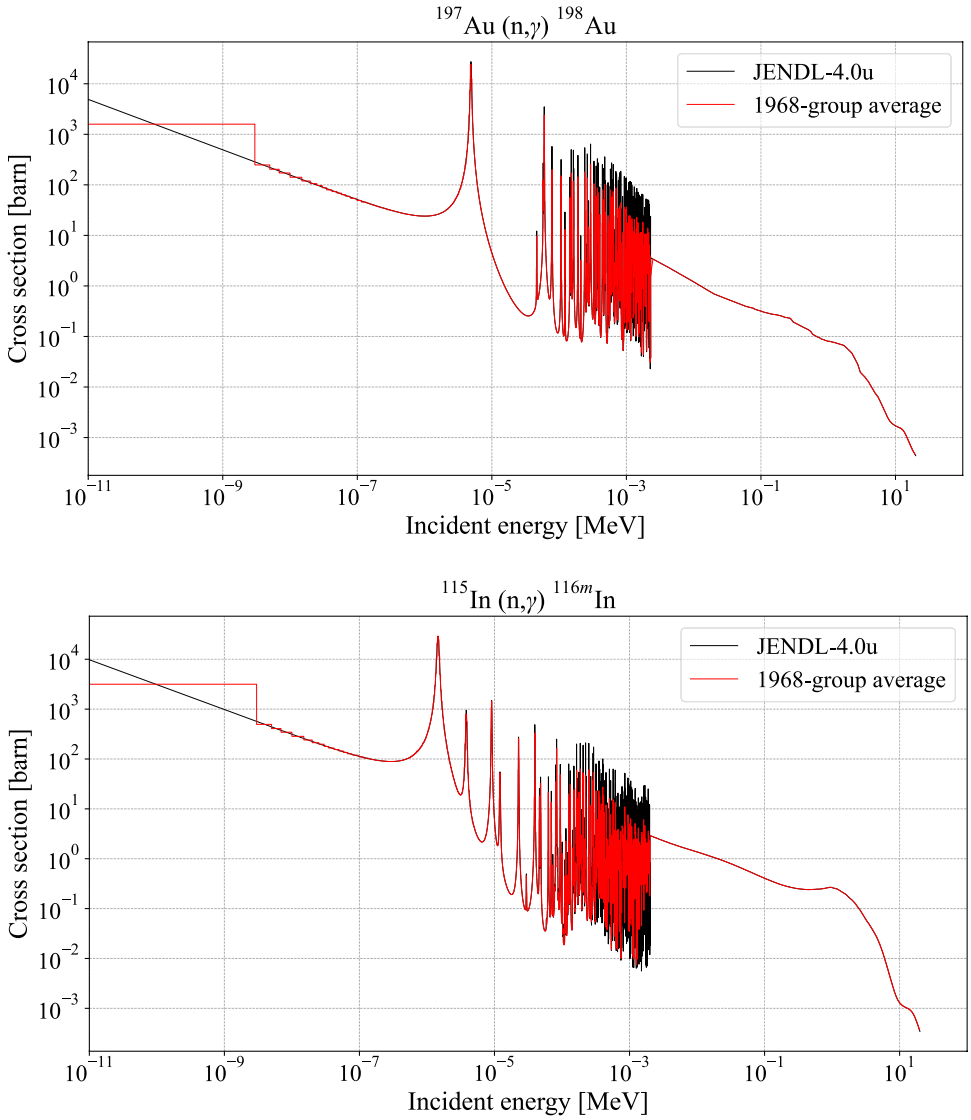

Fig. 8 Neutron energy dependence of the cross section of the reactions ^{197}Au(n, γ)^{198}Au and ^{115}In(n, γ)^{116m}In

Results and discussion

The comparison of the activities between the experimental and the simulated results of both performed activations of ^{197}Au and ^{115}In is shown in Fig. 7. Uncertainties shown include statistical and systematic uncertainties of the experiment. For the simulation, the uncertainty bars are based on systematic uncertainties. Both methods employed for the simulated data show similar results with a systematic trend of estimating lower activity using the DCHAIN than the flux analysis method. This effect can be explained and understood by the difference of how the activity is calculated in the simulations. In the flux analysis, the neutron energy spectrum is separated into neutron energy bins within a 100-group structure between the lowest and the highest energy. However, DCHAIN increases the resolution of the energy spectrum by using a 1968-group structure. This results in an increased computing time, but in a more detailed calculation when folding the energy spectrum with the neutron capture cross section, see Fig. 8. As the different resonance contributions are better resolved in the DCHAIN method, the results may also carry more uncertainty than in the rougher calculations employed by the flux analysis. However, both results agree within 25% in the gold case and within 18% in the indium case.

When comparing the simulation results to the experimental data, the flux analysis slightly overestimates the activity within around 15% in both cases. The DCHAIN analysis conversely underestimates the experimentally derived activity by around 15% for the gold samples, whereas only a very small underestimation is observed in the indium case. Both simulation results are within the

experimental uncertainty of 1σ and systematically show the same deviation in both irradiated foils.

The deviation from a pure 1/E epithermal energy spectrum is expressed by implementation of the α-factor. The good agreement between the simulated results and the experimental data points to a correct treatment of this deviation within the PHITS simulation. Similar α-factors as derived in this work have also been observed in other works [17, 18]. Within our experimental approach, it is not possible to extract the α-factor directly. However, using different experimental methods provided in previous studies [19, 20], it is also possible to derive this factor experimentally, which is a foreseen future work.

Conclusion

Experimentally determined activities of gold and indium foils reached during NAA using an AmBe source were compared to activities derived by two simulation methods employing the PHITS code. We observe good agreement of the activities within experimental uncertainties. As such, the simulation inputs and methods used by PHITS for these kinds of simulations work well and show reliable output. This highlights the possibility of using the PHITS code for a trustable neutron transport simulation and employing it for different scenarios involving neutron transport and activation simulations, as e.g., for the design of various neutron fields required at e.g., accelerator-driven compact neutron sources.

Acknowledgements This research has been financially supported by the German Federal Ministry of Education and Research (BMBF) in the project 99MoBest, funding number 02NUK080B. We also thank Felix Schneider and Uwe Schröer from the University of Applied Sciences Aachen for their support.

Funding Open Access funding enabled and organized by Projekt DEAL.

Declarations

Conflict of interest The authors have no competing interests to declare that are relevant to the content of this article. The authors have no affiliations with or involvement in any organization or entity with any financial interest or non-financial interest in the subject matter or materials discussed in this manuscript. Data sets generated during the current study are available from the corresponding author on reasonable request.

References

1. Brückel T, Gutberlet T, (eds) (2023) Opportunities for research with neutrons at the next generation facility HBS: Overview of the High Brilliance Neutron Source (HBS) technical design report, Vol. 9. Schriften des Forschungszentrums Jülich Reihe Allgemeines / General. Forschungszentrum Jülich, Jülich
2. Anderson IS, Andreani C, Carpenter JM, Festa G, Gorini G, Loong C-K, Senesi R (2016) Research opportunities with compact accelerator-driven neutron sources. Phys Rep 607:1–20. https://doi.org/10.1016/j.physrep.2015.11.002
3. Angelo I, Mario M, Serafina B, Gianfranco C, Vittorio LV, Giulia L, Piera M, Sara V, Federico Z, Domiziano M (2015) Accurate Monte Carlo modeling of cyclotrons for optimization of shielding and activation calculations in the biomedical field. Radiat Phys Chem 116:231–236. https://doi.org/10.1016/j.radphyschem.2015.01.001
4. Jacob GF, Nicolaou G (2018) Optimization of Beam Shaping Assembly design for Boron Neutron Capture Therapy based on a transportable proton accelerator. Alex Eng J 57:2333–2342. https://doi.org/10.1016/j.aej.2017.08.004
5. Johannes B, Eric M, Ulrich R, Paul Z, Thomas G, Thomas B (2023) Technical Design Report HBS Volume 2 – Target Stations and Moderators, Vol. 9. Schriften des Forschungszentrums Jülich Reihe Allgemeines / General. Forschungszentrum Jülich, Jülich. https://doi.org/10.34734/FZJ-2023-03723
6. Doruntin Sh, Ulrich R, Christoph L, Jingjing L, Paul Z, Norberto S, Thomas G (2024) Thomas B (2024) Investigation of the mutual influence of multiple extraction channels for high-current accelerator-based neutron sources. EPJ Web Conf 298:03002. https://doi.org/10.1051/epjconf/202429803002
7. Sato T, Iwamoto Y, Hashimoto S, Ogawa T, Furuta T, Abe S, Kai T, Matsuya Y, Matsuda N, Hirata Y, Sekikawa T, Yao L, Tsai PE, Hunter HN, Iwase H, Sakaki Y, Sugihara K, Shigyo N, Sihver L, Niita K (2024) Recent improvements of the particle and heavy ion transport code system - PHITS version 3.29. J Nucl Sci Technol 61:127–135. https://doi.org/10.1080/00223131.2023.2275736
8. Eberhardt K (2022) Elemental analysis by neutron activation: NAA. In Rösch F (ed) Modern applications, vol. 2, De Gruyter pp. 77–100. https://doi.org/10.1515/9783110742701–003
9. Mirion Technologies (2016) Genie 2000 V3.4.1.– Basic Spectroscopy Software: Detector manual. Mirion Technologies, Canberra
10. Kafala SI (1995) Simple method for true coincidence summing correction. J Radioanal Nucl Chem 191:105–114. https://doi.org/10.1007/BF02035990
11. National Nuclear Data Center (n.d.). Information extracted from the NuDat database. Retrieved from https://www.nndc.bnl.gov/nudat/
12. Shibata K, Iwamoto O, Nakagawa T, Iwamoto N, Ichihara A, Kunieda S, Chiba S, Furutaka K, Otuka N, Ohsawa T, Murata T, Matsunobu H, Zukeran A, Kamada S, Katakura J (2011) JENDL-4.0: A new library for nuclear science and engineering. J Nucl Sci Technol 48:1–30. https://doi.org/10.1080/18811248.2011.9711675
13. Ratliff NH, Matsuda N, Abe S, Miura T, Furuta T, Iwamoto Y, Sato T (2020) Modernization of the DCHAIN-PHITS activation code with new features and updated data libraries. Nucl Instrum Methods Phys Res, B 484:29–41. https://doi.org/10.1016/j.nimb.2020.10.005

14. Van Hung T (2010) Modified method of α determination in the $1/E^{1+\alpha}$ epithermal neutron spectrum of a reactor. J Radioanal Nucl Chem 285:331–336. https://doi.org/10.1007/s10967-010-0549-x
15. Kolotov VP, De Corte F (2004) Compilation of k0 and related data for NAA in the form of an electronic database (IUPAC Technical Report). Pure Appl Chem 76:1921–1925. https://doi.org/10.1351/pac200476101921
16. OECD NEA Data Bank (n.d.) JANIS web. Retrieved from https://www.oecd-nea.org/janisweb/
17. Van Hung T, Sakamoto Y, Yasuda H (1998) Calculation of neutron flux characteristics of Dalat reactor using MCNP4A code (JAERI-Research-98–057). Japan Atomic Energy Research Institute, Tokyo
18. Van Hung T (2010) Determination of the α factor of epithermal neutron flux in Dalat reactor, Vietnam, based on neutron spectrum calculated using MCNP code. J Radioanal Nucl Chem 283:707–711. https://doi.org/10.1007/s10967-010-0457-0
19. Dung H, Cho S (2003) A simple method for α determination. J Radioanal Nucl Chem 257:573–575. https://doi.org/10.1023/a:1025444732641
20. Yücel H, Karadag M (2004) Experimental determination of the α-shape factor in the 1/E1+α epithermal-isotopic neutron source-spectrum by dual monitor method. Ann Nucl Energy 31:681–695. https://doi.org/10.1016/j.anucene.2003.10.002